IEEE Robotics and Automation Letters (RA-L) paper, presented at ICRA 2026, Vienna, Austria. Cite as RA-L paper.

VarWrist: An Anthropomorphic Soft Wrist with Variable Stiffness

Chaozhou Zhang, Min Li, *Member, IEEE*, Zhanshuo Yang, Xiangrui Kong, Jiayi Luo, Yushen Liu, Jian Fu, Guanghua Xu, *Member, IEEE*, and Shan Luo, *Senior Member, IEEE*

***Abstract*—Robotic wrists play a crucial role in enhancing the dexterity and stability of robotic end-effectors. Existing rigid robotic wrists tend to be complex and lack flexibility, while soft robotic wrists often struggle with limited load-bearing capacity and lower accuracy. Human wrists feature multi-degrees of freedom and variable stiffness, which help human hands to accomplish daily tasks. This study presents an innovative anthropomorphic soft robotic wrist, VarWrist, equipped with a fiber jamming variable stiffness module, enabling stiffness adjustment through vacuuming. VarWrist consists of three parallel bellows, utilizing a positive-negative pneumatic actuation strategy to mimic human wrist motion. In addition, the trajectory equation of the rotation center was fitted through modeling. We developed a prototype of VarWrist and assessed its performance. Results indicate that the soft wrist surpasses the motion range of human wrists, achieving flexion (81.9°), extension (78.5°), ulnar deviation (70.5°), and radial deviation (70.5°). The bending motion trajectory showed a 73% increase in similarity to human motion compared to fixed-axis rotation, with VarWrist exhibiting a significant range of variable stiffness (resting state: 206%, working state: 155%). Demonstration experiments confirm that this wrist facilitates a dexterous hand in completing grasping tasks that would be unattainable by the hand alone.**

***Index Terms*—Anthropomorphic wrist, variable stiffness, soft robotics, fiber jamming.**

I. Introduction

In recent years, the development of end-effectors, such as dexterous hands and grippers, has garnered significant attention in the field of robotics. These advancements have enabled some dexterous hands to closely mimic the complex motions of human hands with remarkable flexibility [1]. Importantly, the flexibility and stability of the wrist are essential for executing fine movements and grasping objects in daily life and work [2]. As the human hand performs actions, the wrist facilitates constant posture adjustments, providing critical rotational freedom. Additionally, the wrist supports the hand's weight, enhancing overall stability. Consequently, robotic wrists are crucial for the dexterity and stability of end-effectors, enabling robots to perform complex tasks [3].

The human hand, with its intricate physiological structure, possesses superior grasping capabilities, which the wrist further amplifies by increasing the range of motion (ROM), dexterity, and lifting capacity [4]. Research indicates that human-like designs in robots enhance teleoperation by simplifying control strategies and improving intuitive operation, ultimately reducing cognitive workload and reliance on extensive operational experience [5]. Therefore, the design of robotic wrists should draw inspiration from the human wrist's functionality, considering aspects such as degrees of freedom (DOFs) and range of motion. Notably, the instantaneous rotation centers (IRCs) of wrist joints dynamically change during motion, allowing for a broader ROM, enhanced dexterity, and minimized stress on the wrist [6]. Unfortunately, this dynamic characteristic has not been sufficiently addressed in current robotic wrist research, while studies on lower limb robotics have placed greater emphasis on IRC characteristics in knee joints [7].

Robotic wrists are generally classified into rigid and soft categories. Early rigid wrists, typically motor-driven with fixed mechanical structures, offer stability and precision [8], [9]. However, their complex designs often lack flexibility and adaptability, which are increasingly demanded in unstructured environments. In contrast, soft robots exhibit superior adaptability to external conditions and enhanced human-robot interaction capabilities [10], [11]. For instance, Chen et al. [12] developed a soft wrist by assembling four pneumatic helical actuators, enabling bending and twisting motions. Similarly, Kurumaya et al. [11] created a modular soft wrist using silicone rubber that rotates or bends by injecting gas or water. Nevertheless, these soft wrists often struggle with low stiffness and susceptibility to deformation under external forces, resulting in reduced load capacity [13].

To support and assist end-effectors in various tasks, soft robotic wrists must maintain stable and controllable postures. Therefore, achieving high-stiffness performance and variable-stiffness properties is critical for these systems [14]. Integrating variable stiffness into soft robotic wrists could address this challenge. To date, only a few have explored

Manuscript received December 18, 2024; Revised March 23, 2025; Accepted May 30, 2025. This paper was recommended for publication by Cecilia Laschi upon evaluation of the Associate Editor and Reviewers' comments. This work was supported in part by the National Natural Science Foundation of China under Grant (51975451), Key Research and Development Program of Shaanxi (Program No. 2023-YBGY-353), and Innovation Capability Support Program of Shaanxi (Program No. 2024GH-GHJD-26). (*Corresponding author: Min Li,* e-mail: min.li@mail.xjtu.edu.cn)

C. Zhang, M. Li, Z. Yang, X. Kong, and G. Xu are with the School of Mechanical Engineering, Xi'an Jiaotong University, Xi'an 710049, China. (e-mail: jixiezcz@stu.xjtu.edu.cn; min.li@mail.xjtu.edu.cn; YangZhanshuo@stu.xjtu.edu.cn; kongxr@stu.xjtu.edu.cn; xugh@mail.xjtu.edu.cn).

Jiayi Luo, and Yushen Liu, and Jian Fu are with the Hunan Readore Technology Co., Ltd., China. (e-mail: jiayi.luo@readore.com; yushen.liu@readore.com.cn; fujian@readore.com).

S. Luo is with the Department of Engineering, King's College London, London WC2R 2LS, U.K. (e-mail: shan.luo@kcl.ac.uk).

Digital Object Identifier (DOI): see top of this page.

variable stiffness in soft robotic wrists [15], [16], [17], employing different actuation strategies to adjust stiffness. However, these antagonistic methods require active coupling of the actuators, complicating the achievement of both variable stiffness and positional decoupling [18].

In addition to the antagonistic approach, current techniques for soft robots to achieve variable stiffness include jamming, shape memory materials, and magnetorheological materials [19]. Among these, jamming has gained traction due to its ability to alter stiffness with minimal volume changes, making it a hot research topic in soft robotics [20]. This technique typically involves enclosing solid discrete materials within an elastic membrane. In the absence of jamming, these materials can move freely, providing high flexibility. When a vacuum is applied, the membrane compresses the materials, increasing friction and density, resulting in a transition from liquid-like to solid-like behavior, thereby enhancing overall stiffness [19], [20]. Jamming methods can be further categorized into granular jamming [21], layer jamming [22] and fiber jamming [23], [24]. Fiber jamming avoids the stability and repeatability issues associated with granular rearrangement and the limitations of planar designs in layer jamming. Despite its widespread application in robotics [24], the use of fiber jamming for soft wrists remains unexplored.

In this paper, we propose VarWrist, a pneumatic anthropomorphic soft wrist designed to mimic the human wrist's functionality through variable stiffness. The VarWrist comprises three 3D-printed soft actuators with bellows[1] arranged in parallel, integrated with a central fiber jamming variable stiffness module. These actuators adjust their lengths based on applied positive or negative pneumatic pressure, facilitating bending motions. The variable stiffness module can modify its stiffness through vacuum application. Our contributions are twofold: 1) An anthropomorphic soft wrist driven by three bellows actuators is proposed, which simulates the unfixed rotation center of the human wrist and exhibits a highly biomimetic motion trajectory. 2) For the first time, applying fiber jamming in soft robotic wrists as a solution for effective stiffness variation. Potentially, the robotic wrist developed could be combined with an end-effector for teleoperation tasks. The remainder of this paper is organized as follows: Section II details the design of anthropomorphic wrist. Section III describes performance test experiments. Section IV presents an application scenario demonstration. Section V provides discussions and concludes the paper

II. Design and Fabrication

A. Analysis of Human Wrist and Design Requirements

The human wrist consists of eight bones interconnected by ligaments and the triangular fibrocartilage [25]. This intricate structure facilitates flexible movement, allowing for three degrees of freedom (DOFs): pronation/supination (rotation along the arm's axis, 76°/85°), flexion/extension (rotation toward the palm or back of the hand, 75°/75°), and ulnar/radial deviation (rotation around the carpal axis, perpendicular to the hand, 45°/20°) [3]. Physiological and biomechanical studies show that the human wrist displays variable carpal bone arrangement (see Fig. 1) under different movements due to coordinated radiocarpal and midcarpal joint actions, asymmetric bone arrangement, tendon moment arm variations, and capsule constraints. This unfixed rotation center both evens out load distribution—reducing local joint stress—and enhances movement flexibility and smoothness [25], [26].

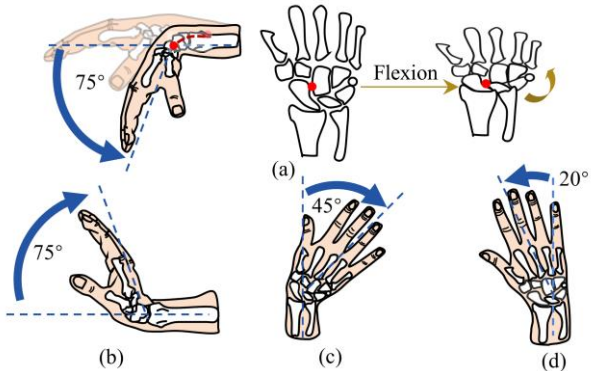

Fig. 1 The human wrist performs (a) flexion, (b) extension, (c) ulnar deviation, and (d) radial deviation movements, during which the arrangement of the carpal bones and the center of rotation undergoes dynamic changes.

Current robotic arms typically employ rotary motors at the wrist to achieve pronation/supination, but they often lack the other two wrist DOFs. Therefore, an effective anthropomorphic wrist design must incorporate flexion/extension and ulnar/radial degrees of freedom while maintaining an unfixed rotation center. Additionally, the wrist must support the weight of the manipulator during tasks. This necessitates a variable stiffness mechanism to adapt to load-bearing requirements across various task conditions.

B. Design and Fabrication of VarWrist

VarWrist, as depicted in Fig. 2(a), features a columnar design with a height of 80 mm and an outer radius of 40 mm. VarWrist integrates bending motion actuators and a variable stiffness module (see Fig. 2(b)). The bending motion actuators consist of three parallel-arranged actuators capable of simulating human wrist movement through pneumatic pressure application. The variable stiffness module adjusts the wrist's stiffness via negative pressure, allowing it to modulate load capacity according to external conditions.

1) Bending Motion Actuators

Three identically structured actuators are arranged in parallel, rotated 120 degrees apart (see Fig. 2(a)). Each actuator features a U-shaped bellow with a hollow chamber, The central area of this constraint layer is hollow to accommodate the variable stiffness module.

Each bellow contains a small opening at its base for air tube insertion. When positive pneumatic pressure is applied, the actuator elongates, while negative pressure causes it to contract. By controlling the pneumatic pressure and the sequence of application to the three bellows, we achieve various deformations that enable VarWrist to perform a range of actions. For instance, Fig. 2(c) shows the wrist performing flexion when actuators I and II are subject to equal negative

[1] A bellows is a type of soft-actuated structure that utilizes a gas-filled cavity to expand and contract, generating motion through changes in air pressure.

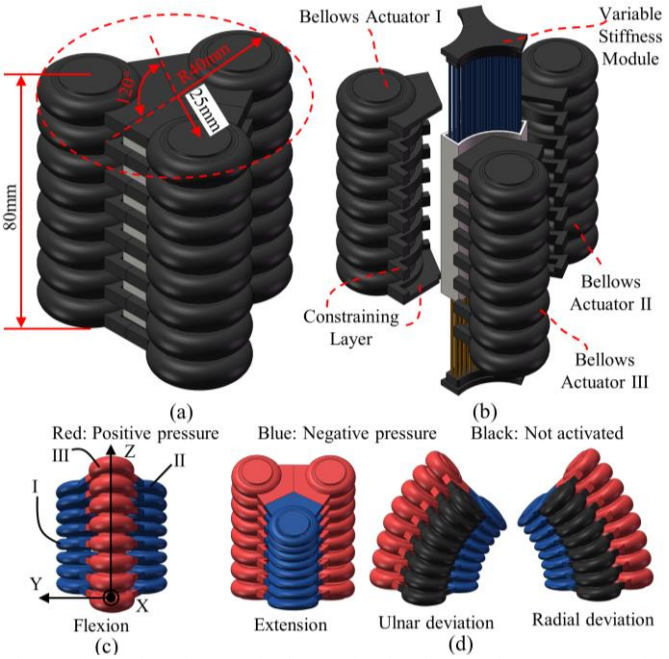

Fig. 2. The design of VarWrist integrating bending motion actuators and a variable stiffness module. (a) Assembly drawing. (b) Explosive view. (c) and (d): The motion of VarWrist under different pressure combinations.

pressure while actuator III receives positive pressure. Similar methods facilitate extension, ulnar/radial deviation, and combinations of these motions, as depicted in Fig. 2(c) - (d).

Notably, as the lengths of the bellows change, the wrist's center of rotation dynamically shifts. In this paper the VarWrist is kinematically modeled based on the classical constant curvature model, to analyze the steady-state bending curvature and center of rotation. The constant curvature model assumes that the actuator has a uniform and constant curvature along the axis at any time [27]. To facilitate a comparative analysis with a fixed center of rotation, a rigid link O_wO_d is constructed with a length equal to the initial length L_0 of VarWrist (where O_w is the equivalent center of rotation and O_d is the center of VarWrist's end). In the resting state of VarWrist, O_w coincides with the origin O. As shown in Fig. 3(a), the three variables $\{\kappa(g),\varphi(g),l(g)\}$ are defined as the curvature, deflection angle and central axis arc length, where $g=\{l_1,l_2,l_3\}$ represents the length of the three actuators.

$$\begin{bmatrix}\kappa(g)\\ \varphi(g)\\ l(g)\end{bmatrix}=\begin{bmatrix}\dfrac{2\sqrt{l_1^2+l_2^2+l_3^2-l_1l_2-l_1l_3-l_2l_3}}{d(l_1+l_2+l_3)}\\ \arctan(\dfrac{\sqrt{3}(l_2-l_3)}{l_2+l_3-2l_1})\\ \dfrac{l_1+l_2+l_3}{3}\end{bmatrix} \quad (1)$$

where d is the distance from the center of the actuator to O_d.

The bending radius $r(g)$ and bending angle $\theta(g)$ are:

$$r(g)=1/\kappa(g) \quad (2)$$

$$\theta(g)=l(g)\kappa(g) \quad (3)$$

Cartesian coordinates for O_d and O_w:

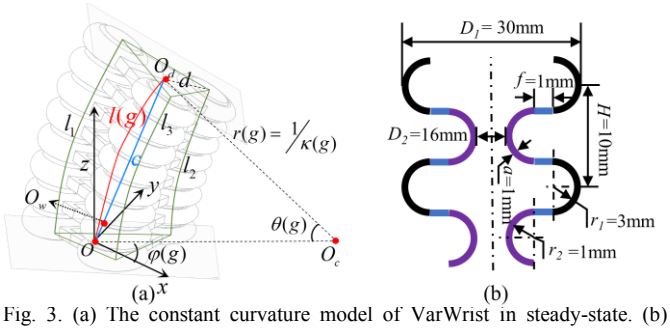

Fig. 3. (a) The constant curvature model of VarWrist in steady-state. (b) Structural parameters of bellows.

$$\left(x_{O_d},\ y_{O_d},\ z_{O_d}\right)=c\left(\sin(\frac{\theta}{2})\cos(\varphi),\sin(\frac{\theta}{2})\sin(\varphi),\cos(\frac{\theta}{2})\right) \quad (4)$$

$$\left(x_{O_w},y_{O_w},z_{O_w}\right)=\left(1-\frac{L_0}{c}\right)\left(x_{O_d},y_{O_d},z_{O_d}\right) \quad (5)$$

where $c=2r(g)\sin(\theta/2)$ is the chord length OO_d.

From (1) ~ (5), it can be observed that by actively adjusting the length differentials of the bellows actuators, the structure achieves dynamic variations in bending curvature and instantaneous center of rotation during movement. Different combinations of bellows lengths are controlled by positive and negative pneumatic pressure. According to studies [28] and [29], the pressure required for different bellows lengths is:

$$P_i=\frac{\left(\dfrac{L_0(l_i-N(r_1+a)/3)}{L_0-N(r_1+a)/3}-L_0\right)k_i}{A} \quad (6)$$

$$l_i=l-\theta d\cos\left(\frac{2\pi}{3}(i-1)+\frac{\pi}{2}-\varphi\right) \quad (7)$$

where N is the number of bellows, r_1 is the inner radius of the bellows (see Fig. 3(b)), a is the thickness of the wall of the bellows, k_i is the stiffness, A is the averaged cross-sectional area of a bellow.

This study specifically analyzes the variations in VarWrist during flexion motion. Since the contraction of actuators I and II can be regarded as a reduction in the initial length L_0, we focus solely on the flexion motion induced by the extension of actuator III:

$$g_1=\{l_1,l_2,l_3\}=\{L_0,L_0,nL_0\} \quad (8)$$

$$\begin{bmatrix}\kappa(g_1)\\ l(g_1)\end{bmatrix}=\begin{bmatrix}\dfrac{2(n-1)}{d(n+2)}\\ \dfrac{(n+2)L_0}{3}\end{bmatrix} \quad (9)$$

where n is the elongation of the actuator III ($1<n<n_{max}$).

In this case, O_w is always located within the XZ-plane. The trajectories of O_d and O_w can be expressed as functions of n:

$$\theta(n)=l(g_1)\kappa(g_1)=\frac{2(n-1)L_0}{3d} \quad (10)$$

$$x_{O_d}(n)=\frac{1-\cos\theta(n)}{\kappa(n)},\ \ z_{O_d}(n)=\frac{\sin\theta(n)}{\kappa(n)} \quad (11)$$

$$\begin{aligned}x_{O_w}(n)&=\frac{1-\cos\theta(n)}{\kappa(n)}-\frac{1-\cos\theta(n)}{2\sin(\theta/2)}L_0\\ z_{O_w}(n)&=\frac{\sin\theta(n)}{\kappa(n)}-\cos(\frac{\theta}{2})L_0\end{aligned} \quad (12)$$

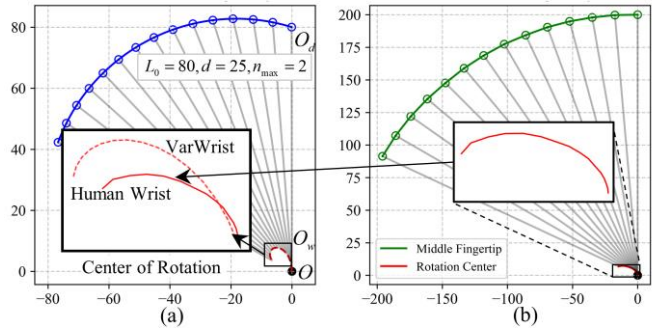

Fig. 4. The end-effector and the rotation center trajectories of (a) calculated using the proposed model and (b) the human wrist during flexion motion.

Fig. 4(a) illustrates the trajectories of the rotation center O_w and the end-center O_d of VarWrist during flexion motion. To enhance the anthropomorphic characteristics of VarWrist, the rotation center's trajectory was optimized to match that of the human wrist. We measured the flexion motion trajectory of the middle fingertip using a coordinate paper calibration method. Based on the measured data, the trajectory equation of the rotation center (x_{human}, z_{human}) during human wrist flexion was calculated and fitted (see Fig. 4(b)):

$$z_{human} = -0.0836x_{human}^2 - 1.4659x_{human} + 0.74387 \quad (13)$$

Thus, this study first establishes preliminary structural parameters for the VarWrist based on the desired range of motion (1), (6), (7). Trajectory fitting error (11) is then adopted as the optimization target, with a grid search approach applied to adjustment the parameters, followed by integer rounding to determine the final parameter set. This approach ensures both functional compliance with motion requirements and enhanced biomimetic performance through trajectory optimization.

$$E(\omega) = \sum_{i=1}^{12} \left\| \begin{pmatrix} x_{O_w}(n_i;\omega) \\ z_{O_w}(n_i;\omega) \end{pmatrix} - \begin{pmatrix} x_{human}(n_i) \\ z_{human}(n_i) \end{pmatrix} \right\|^2 \quad (14)$$

where ω is the optimization parameter.

The bellows were fabricated using a 3D printer (E2, Raise3D) with flexible materials (83A TPE, eSUN), printed horizontally. Printing parameters were optimized to ensure proper sealing, as shown in Table I.

TABLE I
PRINTING PARAMETERS FOR ACTUATORS WITH BELLOWS

Parameter	Value	Parameter	Value
Layer height (mm)	0.1	Shell thickness (mm)	1.2
Fill density (%)	100	Extruder temperature (C°)	230
Platform temperature (C°)	50	Print speed (mm/s)	20
Infill speed (mm/s)	20	Inner shell speed (mm/s)	10
Outer shell speed(mm/s)	10	First layer speed (mm/s)	10

2) Variable Stiffness Module

The design and operational principles of the variable stiffness module are illustrated in Fig. 5. Comprising multiple fibers, an elastic membrane, and end plates (see Fig. 5(a) and (b)), this module utilizes negative pneumatic pressure to enhance stiffness. The applied pressure compresses the elastic membrane against the internal fibers, significantly increasing friction and immobilizing their movement, which effectively raises the module's stiffness. The triangular shape of the variable stiffness module maximizes fiber accommodation, thereby increasing its stiffness potential.

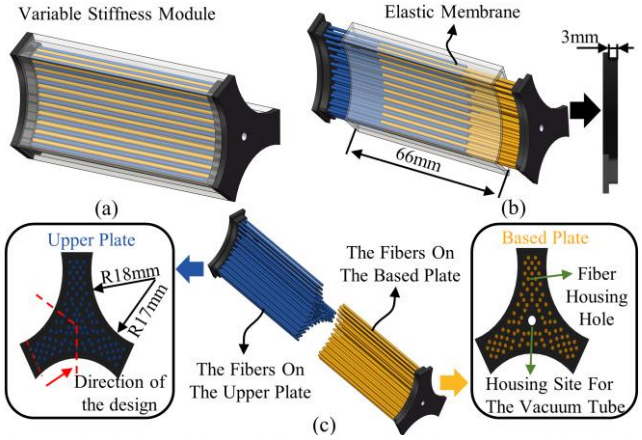

Fig. 5. The design of the variable stiffness module. (a) Assembly drawing. (b) Explosive view. (c) Parameters of the two plates and fiber setting.

Based on research [23], a comb-type (CT) fiber arrangement offers superior stiffness compared to bundle-type (BT) and fixed bundle-type (FBT) designs. Our design incorporates this CT arrangement (see Fig. 5(c)). The triangular end plates feature multiple holes, arranged in staggered rows, to secure the fibers. Various materials can be utilized as filling fibers, including polytetrafluoroethylene (PTFE), polyvinyl chloride (PVC), Nylon, silicone, and leather. Brancadoro et al. [24] found that waxed cotton provides a broad range of stiffness variation, but its stiffness post-adjustment is insufficient for significant actuator deformations. Conversely, Nylon offers the highest absolute stiffness, leading us to select nylon wires (TCNL100, EOONGSNG) with a diameter of 1 mm as the filling fibers. The holes in the triangular plates match this diameter, with 99 holes in the upper plate and 87 in the base plate.

The fabrication process for the variable stiffness module is depicted in Fig. 6. Initially, we designed and assembled molds, including mold I, mold II, mold core, and a locator. After applying a release agent (MS-606, BEAUTREE) on the mold surfaces, we poured prepared silicone (Ecoflex 00-30, Smooth-On) into the mold. To achieve a homogeneous elastic membrane, we placed the mold in a vacuum chamber to eliminate air bubbles. After 8 to 10 hours, the silicone cured. Subsequently, nylon filaments, cut into 63 mm segments, were

Fig. 6. Fabricating process of the variable stiffness module.

heat-treated for straightening. The straightened fibers were inserted into the triangular plates' holes and secured with adhesive. The upper and base plates were interspersed to form a CT fiber arrangement, and the elastic membrane was wrapped around the outer layer. Finally, the elastic membrane was adhered to the plates' convex platform, completing the module's fabrication. The molds and plates were 3D printed using a Raise3D E2 printer with PLA filament.

C. Control System

The control module is designed to regulate both the bending motion actuators and the variable stiffness module. As illustrated in Fig. 7, a personal computer (PC) communicates with each component via an analog input and output module (JY-DAM10AIAO, JVYING ELECTRONIC). An air compressor (U-601G, USTAR) and a vacuum pump (VP-15S, JOANLAB) provide positive and negative pressures, respectively. Three compact electro-pneumatic regulators (ITV0030-2BL, SMC) control the positive pressure for the actuators, while three additional regulators (ITV0090-2BS, SMC) manage the negative pressure. A separate regulator controls the vacuum for the variable stiffness module. Three pulse-triggered switches and three 3-port solenoid valves (VT307V-6G1-02, SMC) switch the air paths to deliver positive or negative pneumatic pressure to the actuators. Upon receiving a control command from the PC, VarWrist executes a bending motion, followed by the activation of the variable stiffness module to enhance overall stiffness.

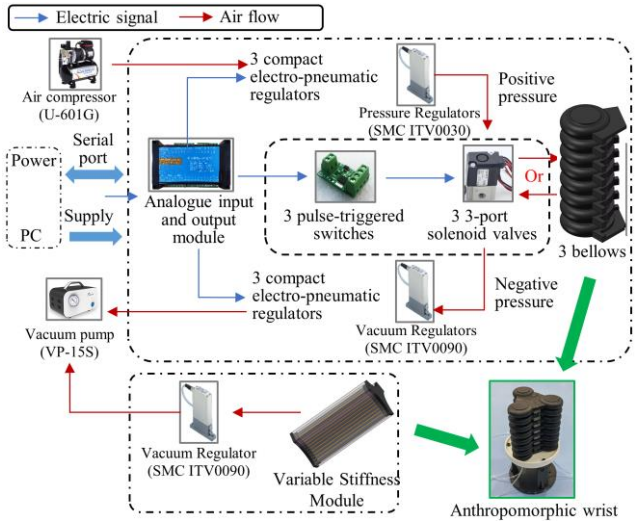

Fig. 7. System integration of the prototype containing the wrist prototype and the control module.

III. Experimental Characterization

Characterization experiments were conducted to evaluate the ROM, motion trajectory, and variable stiffness of VarWrist.

A. Weight and Dimensions

VarWrist weighs 78.7 g, which is lighter than the wrist mass of an adult (100 - 150 g). And the outer diameter is 80mm, larger than the average adult male wrist diameter of about 57.3mm.

B. Range of Motion

The ROM evaluation involved measuring flexion/extension and ulnar/radial motions of VarWrist. Two IMU sensors (JY901, Wit-motion) were strategically positioned at the top and bottom of the wrist (see Fig. 8(a)). The angle between the sensor planes was recorded, with the bottom sensor serving as a reference. The wrist's flexion/extension motion is facilitated by the interaction of three bellows actuators. In the flexion experiment, identical negative pressures (0, -20 kPa, -40 kPa, and -60 kPa) were applied to actuators I and II, while actuator III received positive pressure ranging from 0 to 200 kPa in 10 kPa increments. Conversely, for extension, opposite pressures were applied. Ulnar deviation involved actuator I shortening in tandem with actuator II elongating while maintaining actuator III's pressure at zero, enabling wrist rotation around the y-axis. Each experimental condition was repeated five times.

The resulting flexion/extension angle curves (see Fig. 8(b) and (c)) showed that the synergistic application of positive and negative pressures effectively expanded the wrist's ROM. The maximum flexion and extension angles achieved were 81.94° and 78.47°, respectively, exceeding the human wrist's maximum angles of 75°. As deformation increased, the slope of the bending curve diminished. This aligns with the predicted trend of the model and indicates rising stiffness in the actuators, which affected wrist motion. In Fig. 8(d), the orange lines represent the positive and negative pressure combinations that produce pure ulnar deviation. Under other pressure combinations, ulnar deviation is accompanied by flexion-extension motion, as indicated by the green region. The maximum recorded ulnar deviation angle was 70.53°, surpassing the human wrist's limit of approximately 45°.

C. Motion Trajectory

VarWrist wrist's motion trajectory was evaluated for its biomimetic properties. A dexterous hand [30] with a length of 205 mm and a weight of 356 g was mounted on VarWrist to form a robotic forearm. Marker points were placed at the

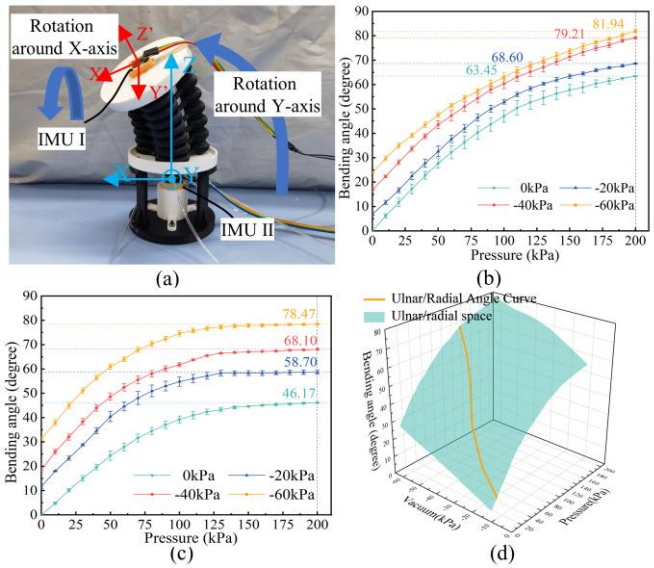

Fig. 8. Range of motion experiment: (a) the experimental set-up, (b) and (c) the flexion and extension angle curves, (d) the results of ulnar deviation.

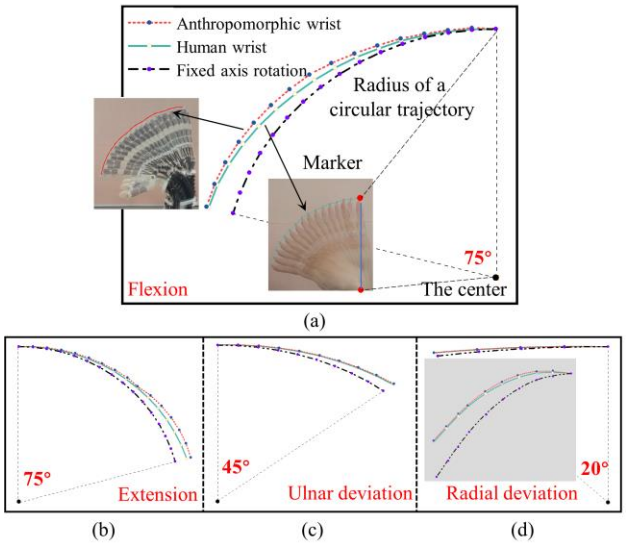

Fig. 9. Motion trajectories of the middle fingertip during the VarWrist movements: (a) flexion, (b) extension, (c) ulnar / (d) radial deviation.

middle fingertip of both the robotic and human hands, and their movements were captured via video. VarWrist performed bending motion while the hand maintained its shape, allowing for trajectory analysis at 5° increments of flexion.

The plotted motion trajectories of both forearms within a coordinate system (see Fig. 9) were adjusted for alignment. A circular trajectory with a fixed-axis rotation was included for comparison. The results indicated that the motion trajectories of the robotic forearm closely mirrored those of human wrist.

To quantitatively analyze trajectory similarity, Euclidean distances R_i were calculated between corresponding sampling points of human wrist trajectory and the other two trajectories:

$$R_i = R(t_i, w_i) = \|t_i - w_i\| \tag{15}$$

where i indicates sampling points, range from 0 - 16; t_i and w_i indicates points on two trajectories. The root-mean-square for all sampled points in each trajectory was calculated.

TABLE II
DEVIATION OF THE MOTION TRAJECTORY WITH HUMAN WRIST

	Flexion	Extension	Ulnar deviation	Radial deviation
Fixed-axis rotation (mm)	10.07	7.89	6.46	2.50
VarWrist (mm)	3.41	3.66	0.64	0.20
Improvement (%)	66.14	53.61	90.10	82.14

As shown in Table II, the motion trajectories of VarWrist achieved an average improvement of 73% compared to fixed-axis rotations. Notably, the larger deviation of the flexion/extension trajectory is due to the larger angle of motion. In addition, Table II indicates that the ulnar/radial deviation trajectory of the VarWrist closely mimics natural wrist movement. The enhanced similarity may stem from the distinct motion properties in the two perpendicular directions.

D. Variable Stiffness

Separate tests assessed the stiffness of both the variable stiffness module and the VarWrist under varying conditions.

1) Variable Stiffness Module

The setup for measuring the stiffness of the variable stiffness module is depicted in Fig. 10(a). The force exerted are measured using a 6-axis Force/Torque sensor (Nano17, SI-12-0.12, USA). The sensor's range is 0-17 N with a resolution of 0.003 N. The slider advanced 30 mm at 2 mm/s and retracted, allowing for stiffness evaluation at various pressures (-20, -40, -60 kPa), with each condition tested five times.

The results indicated that increased negative pressure correlated with higher stiffness (see Fig. 10(e)). At -60 kPa, the module's stiffness was 14 times greater than at 0 kPa. Forces recorded at 30 mm deflection were 1.93 N under 0 kPa and 14.85 N under -60 kPa, confirming the module's significant absolute stiffness. Notably, during retraction, the module exhibited a sharp decline in force due to its retained deformed shape, leading to a loss of contact with the sensor.

2) Anthropomorphic Wrist

The experimental setup for evaluating the anthropomorphic wrist's stiffness is illustrated in Fig. 10 (b). Stiffness variations of the wrist in both resting and working states were assessed (see Fig. 10(c) and (d)). The protocol mirrored that of the variable stiffness module, except a BSLM-2 sensor (BUFSON, range 0-100 N, resolution 0.02 N) was used. In the resting state, all actuators maintained 0 kPa pressure. In the working state, actuator I was pressurized to 100 or 200 kPa while the others remained at -20 kPa or -40 kPa. During the experiment, VarWrist first performed a bending motion, followed by stiffness modulation. Meanwhile, we recorded the time required for the stiffness module to take effect using the feedback from the pneumatic regulator (ITV0090-2BS).

The effect of the variable stiffness module on the wrist's overall stiffness is shown in Fig. 10(f). Consistent with the trend observed in the module alone, the wrist's stiffness

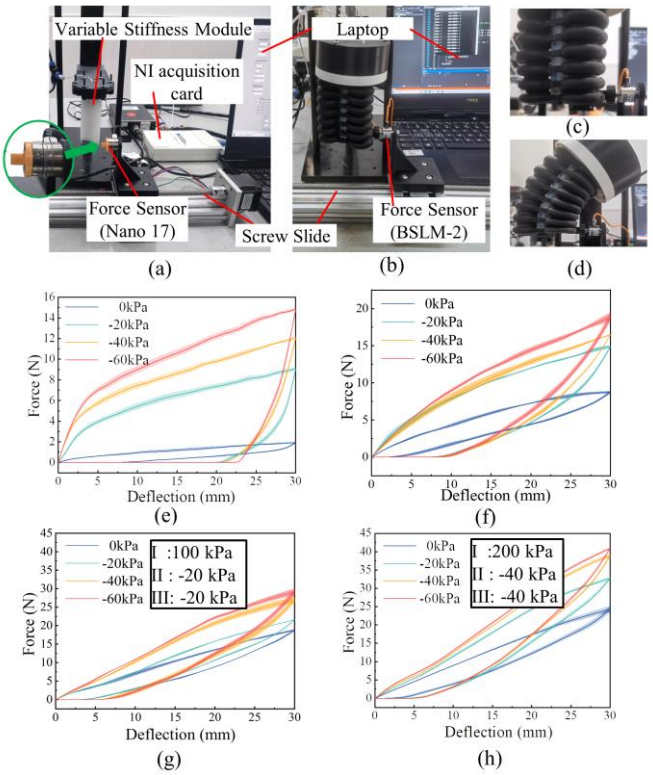

Fig. 10. Stiffness experimental set-up for (a) variable stiffness module and (b) – (d) VarWrist. Results showing stiffness for (e) the variable stiffness module; (f) VarWrist at rest; (g) – (h) VarWrist in a working state.

increased as negative pressure was applied, reaching a 2.06-fold (206%) increase at -60 kPa, with a maximum resistance of 18.87 N at a 30 mm deflection. Although the wrist's resistance was slightly elevated, the hysteresis and shape-locking effects were slightly reduced, likely due to the inherent stiffness of the bellows actuators. Fig. 10(g) and (h) depicts the stiffness behavior of the wrist in the working state, showing a maximum stiffness increase of 1.78 times. Under these conditions, the wrist achieved a maximum force of 40.93 N, highlighting its enhanced performance. The transition time for the variable stiffness module from the resting state to the working state at -60 kPa is 0.79s ± 0.14s. Additionally, the stiffness modulation effect becomes more pronounced as the VarWrist bends, which may be attributed to more significant friction effects between fibers during bending of the actuator.

IV. Demonstration of an Application Scenario

To evaluate the functionality of VarWrist, we constructed a potential application scenario that highlights its ability to enhance the dexterous hand's reach and stiffness adjustment capabilities. As shown in Fig. 11(a), the setup involved a ball suspended within a box by a rope, featuring a single narrow vertical entryway measuring 300×130 mm, which was the sole access point for the robotic forearm. The target suspension points of the ball were offset by 130 mm from the entrance. During the grasping process, the robotic forearm was inserted vertically into the narrow channel. The anthropomorphic wrist's bending motion with an unfixed rotation center enabled the dexterous hand to reach the optimal grasping position (see Fig. 11(b)). After successfully grasping the ball, the wrist extended and straightened (see Fig. 11(c)), while activating the variable stiffness module increased the wrist's loading capacity. This enhancement allowed the robotic forearm to withdraw the ball from the channel. As shown in Fig. 11(d), manipulating only the dexterous hand does not allow it to reach the grasping position. Additionally, without the variable stiffness feature, the wrist bends under load, preventing it from retrieving the ball from the hole (see Fig. 11(e)). A program script was developed to execute this task, and the VarWrist successfully completed three consecutive trials. These results effectively demonstrate the VarWrist's potential in scenarios requiring flexible motion and adjustable stiffness, showcasing its practical application in complex tasks.

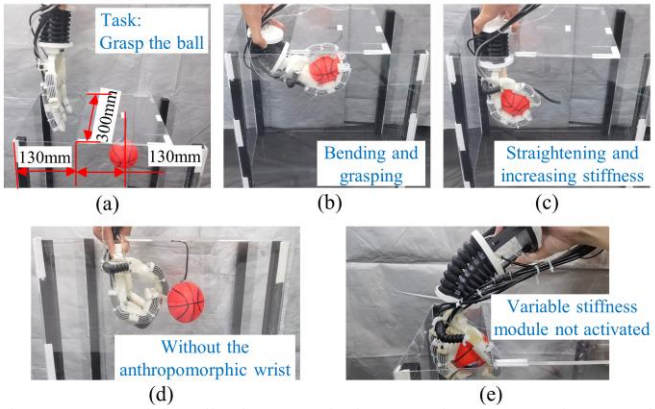

Fig. 11. A potential application scenario for VarWrist: (a) Scenario setup. (b) and (c) Successful completion of the task. Without VarWrist (d) and stiffness module (e) cannot complete the task.

V. Discussion and Conclusion

A. Discussion

Table III highlights the comparative performance of the proposed VarWrist against other robotic wrists in terms of actuator type, DOFs, weight, ROM, and variable stiffness. Although the ROM of VarWrist is slightly smaller than that of some designs, such as those in [12] and [16], it still exceeds the natural ROM of the human wrist. Moreover, VarWrist achieves superior absolute stiffness and reduced weight compared to other designs, demonstrating a well-balanced performance across key metrics.

TABLE III
Comparison with Other Soft Robotic Wrists

Reference	DOFs	Weight	ROM (F^1, E^2, R^3, U^4; T^5)	Variable stiffness (Range; Resisting force)
Our VarWrist	2	78.7 g	81.9°,78.5°,70.5°,70.5°; –	P^6, 206% (-60~0 kPa); 40.93 N
Motor cable [9]	2	1110 g	55°,45°,48°,48°;180°	Elastic Elements, 300%; –
Pneumatic [11]	3	–	122°,122°,122°,122°; 90°	–
Pneumatic [16]	2	389 g	88.2°,90.8°,72.3°,48.6°; –	P^6, 307% (0~120 kPa); 16.00 N
Motor cable[15]	2	160 g	Close to human wrist; –	P^6, 170% (0~90 kPa); 4.23 N
SMA [17]	2	50 g	53°,50°,40°,42°; -	SMA, 1000%; >1 kg

[1] F, Flexion; [2] E, Extension; [3] R, Radial deviation; [4] U, Ulnar deviation; [5] T, Twisting (Pronation/supination); [6] P, Pneumatic.

Current research on pneumatic soft robotic wrists primarily emphasizes achieving 3 DOFs [12]. While designs like the one in [31] employ a similar three-bellows structure with kinematic modeling, their load-bearing capacity is limited (e.g., 110 g) due to the absence of variable stiffness. Among existing designs, only three wrists integrate variable stiffness mechanisms. Hu et al. [32], for instance, developed a six-actuator wrist using particle jamming, which is relatively bulky (diameter: 139 mm, height: 111.2 mm). In contrast, VarWrist incorporates a novel fiber jamming-based variable stiffness module within the three-parallel bellows system (diameter: 80 mm, height: 80 mm), achieving a stiffness increase of 2.06 times compared to non-variable stiffness designs. With a maximum resisting force of 40.93 N, it significantly outperforms other variable stiffness wrists and exceeds prior fiber jamming systems [23] by delivering a maximum stiffness increase over 14 times the original level. The properties of the filler material, dimensions, and density within the variable stiffness module play a crucial role in determining friction and stiffness [23], [24]. Future work should focus on further modeling and analyzing the mechanism of fiber jamming variable stiffness.

At present, the transition of the variable stiffness module occurs within 1s. Optimizing the pneumatic circuit could further improve the response speed of stiffness adjustment [33]. Future work should integrate a closed-loop control system with fuzzy control algorithms to enable real-time adaptive stiffness adjustment during wrist motion.

Kinematic modeling reveals that positive/negative pressure control enables different length combinations of the three bellows, thereby achieving varying bending curvatures and dynamic changes in the center of rotation. Additionally, the

parameter of the VarWrist is selected based on trajectory optimization and range of motion using the grid search method. Experimental results confirm that the motion trajectories of VarWrist closely mimic natural human wrist movement, providing a 73% improvement in trajectory accuracy over fixed-axis designs. This natural motion alignment, coupled with variable stiffness capabilities, offers promising enhancements in load-carrying capacity. Future work should incorporate other parameters optimization algorithms to further enhance the material properties of the bellows and fibers, with the goal of reducing the size of the wrist and optimizing the overall motion space. And we consider actuating VarWrist solely through negative pressure to simplify the control system. Additionally, research on compliant control algorithms for multi-actuator systems utilizing positive and negative pressure remains underexplored, warranting further investigation. And we will further explore the advantages in teleoperation applications.

B. Conclusion

In this study, we proposed a pneumatic anthropomorphic soft wrist, VarWrist, featuring an unfixed rotation center and adjustable stiffness, mimicking human wrist functions for flexion/extension, ulnar/radial deviation, and their compound movements. Comprising three parallel bellows actuators and a centrally located variable stiffness module, the wrist's bending motion is controlled through varying positive and negative pressures. The innovative fiber jamming mechanism, utilizing a comb-type arrangement, enabled substantial stiffness variation. Experimental results demonstrated that our wrist exceeds the ROM of the human wrist (flexion/extension: 81.9°/78.5°, ulnar/radial deviation: 70.5°/70.5°), and its bending trajectory showed a 73% increase in similarity to human motion compared to fixed-axis rotation. This soft wrist, in conjunction with an end-effector, holds significant potential for future teleoperation applications.

REFERENCES

[1] T. H. Wang, T. Jin, Q. Zhang, *et al.*, "A Bioinspired Gripper with Sequential Motion and Mutable Posture Enabled by Antagonistic Mechanism," *Adv. Intell. Syst.,* vol. 5, no. 3, MAR, 2023.

[2] S. Durand, C. P. Y. Rohan, T. Hamilton, W. Skalli, and H. I. Krebs, "Passive Wrist Stiffness: The Influence of Handedness," *IEEE Trans. on Biomed. Eng.,* vol. 66, no. 3, pp. 656-665, 2019.

[3] N. M. Bajaj, A. J. Spiers, and A. M. Dollar, "State of the Art in Artificial Wrists: A Review of Prosthetic and Robotic Wrist Design," *IEEE Trans. on Robot.,* vol. 35, no. 1, pp. 261-277, 2019.

[4] G. Lee, G. Y. Hong, *et al.*, "Tendon-Driven Compliant Prosthetic Wrist Consisting of Three Rows Based on the Concept of Tensegrity Structure," *IEEE Robot. and Automation Letters,* vol. 6, no. 2, pp. 3956-3963, 2021.

[5] J. Molnar, V. Agrawal, and S. Chernova, "Clustering user preferences for personalized teleoperation control schemes via trajectory similarity analysis," *Frontiers in Robot. and Ai,* vol. 11, APR 9, 2024.

[6] B. Akhbari, A. M. Morton, K. N. Shah, J. Molino, D. C. Moore, A. P. C. Weiss, S. W. Wolfe, and J. J. Crisco, "Proximal-distal shift of the center of rotation in a total wrist arthroplasty is more than twice of the healthy wrist," *J. of Orthopaedic Res.,* vol. 38, no. 7, pp. 1575-1586, JUL, 2020.

[7] K. J. Kim, M. S. Kang, *et al.*, "Conceptualization of an exoskeleton Continuous Passive Motion(CPM) device using a link structure," in *2011 IEEE Int. Conf. on Rehabil. Robot. (ICORR)*, 2011.

[8] Y. F. Lee, *et al.*, "A Humanoid Robotic Wrist With Two-Dimensional Series Elastic Actuation for Accurate Force/Torque Interaction," *IEEE/ASME Trans. on Mechatronics,* vol. 21, no. 3, pp. 1315-1325, 2016.

[9] G. Milazzo, M. G. Catalano, A. Bicchi, and G. Grioli, "Modeling and Control of a Novel Variable Stiffness Three DoFs Wrist," *Int. J. of Robot. Res.,* vol. 43, no. 12, pp. 1898-1915, OCT, 2024.

[10] C. Laschi, B. Mazzolai, and M. Cianchetti, "Soft robotics: Technologies and systems pushing the boundaries of robot abilities," *Sci. Robot.,* vol. 1, no. 1, pp. eaah3690, 2016.

[11] S. Kurumaya, B. T. Phillips, *et al.*, "A Modular Soft Robotic Wrist for Underwater Manipulation," *Soft Robot.,* vol. 5, no. 4, pp. 399-409, 2018.

[12] G. Chen, T. Lin, S. Ding, *et al.*, "Design and Test of an Active Pneumatic Soft Wrist for Soft Grippers," *Actuators,* vol. 11, no. 11, pp. 311, 2022.

[13] P. Wang, Z. Tang, W. Xin, *et al.*, "Design and Experimental Characterization of a Push-Pull Flexible Rod-Driven Soft-Bodied Robot," *IEEE Robot. and Automation Letters,* vol. 7, no. 4, pp. 8933-8940, 2022.

[14] I. Onda, K. Tadakuma, M. Watanabe, K. Abe, T. Watanabe, M. Konyo, and S. Tadokoro, "Highly Articulated Tube Mechanism With Variable Stiffness and Shape Restoration Using a Pneumatic Actuator," *IEEE Robot. and Automation Letters,* vol. 7, no. 2, pp. 3664-3671, 2022.

[15] W. Chen, J. Zhou, *et al.*, "Tele-Operated Oropharyngeal Swab (TOOS) Robot Enabled by TSS Soft Hand for Safe and Effective Sampling," *IEEE Trans. on Med. Robot. and Bionics,* vol. 3, no. 4, pp. 1040-1053, 2021.

[16] Y. Fei, J. Wang, and W. Pang, "A Novel Fabric-Based Versatile and Stiffness-Tunable Soft Gripper Integrating Soft Pneumatic Fingers and Wrist," *Soft Robot.,* vol. 6, no. 1, pp. 1-20, 2019.

[17] K. Hyeon, C. Chung, J. Ma, and K. U. Kyung, "Lightweight and Flexible Prosthetic Wrist With Shape Memory Alloy (SMA)-Based Artificial Muscle and Elliptic Rolling Joint," *IEEE Roboti. and Automation Letters,* vol. 8, no. 11, pp. 7849-7856, 2023.

[18] W. Q. Dou, G. L. Zhong, J. L. Cao, Z. Shi, B. W. Peng, and L. Z. Jiang, "Soft Robotic Manipulators: Designs, Actuation, Stiffness Tuning, and Sensing," *Advanced Materials Technologies,* vol. 6, no. 9, Sep, 2021.

[19] M. Manti, V. Cacucciolo, and M. Cianchetti, "Stiffening in Soft Robotics: A Review of the State of the Art," *IEEE Robot. & Automat. Mag.,* vol. 23, no. 3, pp. 93-106, 2016.

[20] S. G. Fitzgerald, G. W. Delaney, and D. Howard, "A Review of Jamming Actuation in Soft Robotics," *Actuators,* vol. 9, no. 4, pp. 104, 2020.

[21] Y. Li, Y. Chen, Y. Yang, and Y. Wei, "Passive Particle Jamming and Its Stiffening of Soft Robotic Grippers," *IEEE Trans. on Robot.,* vol. 33, no. 2, pp. 446-455, 2017.

[22] T. Wang, J. Zhang, Y. Li, J. Hong, and M. Y. Wang, "Electrostatic Layer Jamming Variable Stiffness for Soft Robotics," *IEEE/ASME Trans. on Mechatronics,* vol. 24, no. 2, pp. 424-433, 2019.

[23] M. Brancadoro, M. Manti, S. Tognarelli, and M. Cianchetti, "Fiber Jamming Transition as a Stiffening Mechanism for Soft Robotics," *Soft Robot.,* vol. 7, no. 6, pp. 663-674, Dec, 2020.

[24] M. Brancadoro, M. Manti, *et al.*, "Preliminary experimental study on variable stiffness structures based on fiber jamming for soft robots." in *2018 IEEE Int. Conf. on Soft Robot. (RoboSoft)*, pp. 258-263.

[25] R. Badida, B. Akhbari, *et al.*, "The role of scapholunate interosseous, dorsal intercarpal, and radiolunate ligaments in wrist biomechanics," *J. of Biomechanics,* vol. 125, pp. 110567, 2021/08/26/, 2021.

[26] H. Moritomo, T. Murase, *et al.*, "In vivo three-dimensional kinematics of the midcarpal joint of the wrist," *J. of Bone and Joing Surgery-American Volume,* vol. 88A, no. 3, pp. 611-621, MAR, 2006.

[27] B. A. Jones, and I. D. Walker, "Kinematics for multisection continuum robots," *IEEE Trans. on Robot.,* vol. 22, no. 1, pp. 43-55, 2006.

[28] A. Jonsson and M. Hermann, "Static characteristics of flexible bellows," ¨ master's thesis, Dept. Mech. Eng., Blekinge Inst. Technol., Karlskrona, Sweden, 1997.

[29] D. Drotman, M. Ishida, *et al.*, "Application-Driven Design of Soft, 3-D Printed, Pneumatic Actuators With Bellows," *IEEE/ASME Transactions on Mechatronics,* vol. 24, no. 1, pp. 78-87, 2019.

[30]C. Zhang, M. Li, *et al.*, "An Anthropomorphic Robotic Hand With a Soft-Rigid Hybrid Structure and Positive- Negative Pneumatic Actuation," *IEEE Robotics and Automation Letters,* vol. 8, no. 7, pp. 4346-4353, 2023.

[31] J. Liang, X. Huang, K. Luo, Z. Song, Y. Yang and F. Chen, "Design and Kinematic Modeling of a Pneumatic Soft Bellow-Type Wrist," *IEEE Robot. and Automation Letters*, vol. 9, no. 7, pp. 6312-6319, July 2024.

[32] Hu, T., Lu, X., *et al.*, "Biomimetic soft robotic wrist with 3-DOF motion and stiffness tunability based on ring-reinforced pneumatic actuators and a particle jamming joint," *Sci. China Technol. Sci.* 67, 774–790, 2024.

[33] S. Jadhav, M. R. A. Majit, *et al.*, "Variable Stiffness Devices Using Fiber Jamming for Application in Soft Robotics and Wearable Haptics," *Soft Robot.,* vol. 9, no. 1, pp. 173-186, 2022/02/01, 2021.